Microelectronic Engineering 88 (2011) 1939–1943

Contents lists available at ScienceDirect

Microelectronic Engineering

journal homepage: www.elsevier.com/locate/mee

Effect of upper surface characteristics on meniscus stability in immersion flow field

Ying Chen [a], Kok-Meng Lee [b,1], Xin Fu [a,*]

[a] The State Key Laboratory of Fluid Power Transmission and Control, Zhejiang University, Hangzhou 310027, China
[b] George W. Woodruff School of Mechanical Engineering, Georgia Institute of Technology, Atlanta, GA 30332-0405, USA

ARTICLE INFO

Article history:
Available online 16 February 2011

Keywords:
Immersion lithography
Meniscus stability
Liquid loss
Dynamic model
Immersion unit

ABSTRACT

Liquid loss occurs at the receding contact line when scanning at high speeds resulting in defects on printed patterns in immersion lithography. To offer intuitive insights into the dynamic effects of the fluid confined between the lens and substrate on critical scan speeds, image processing techniques are explored to develop dynamic models for optimizing future designs of immersion units. Since the distance between the last lens and wafer is less than 1 mm, the dynamic characteristics of the liquid (with free boundary and characteristics of the upper surface of the flow field) play an important role in liquid control, which is concerned in various potential immersion unit designs. A method for characterizing the meniscus dynamics is developed to analyze the liquid behavior and meniscus stability in immersion lithography. A second-order system model is presented to better understand the meniscus development during scanning motion. Experimental results have shown that the meniscus adhering to the hydrophilic surface allows for a higher scanning speed than that adhering to the hydrophobic surface.

1. Introduction

Immersion lithography improves optical resolution to 45 nm and below without much change in technical infrastructure. To increase the refraction index in the space between the projection lens and substrate, liquid with high refractive index is injected in place of the low refractive index gas that currently fills the gap [1]. Motivated by the interest to increase production throughputs in semiconductor industry, wafers are scanned at higher and higher velocity and acceleration.

In typical immersion lithography, the liquid (provided by an immersion liquid control system that keeps the liquid fresh and clean to prevent deposition of contaminations) must be confined by an immersion unit within the gap beneath the exposure area [2] while the wafer moves at high speeds. Liquid loss occurred at the receding contact line as well as impurities deposited on the substrate with residual droplets evaporating often result in defects on printed patterns [3]. The meniscus stability depends on the scan speed, the viscosity and surface tension of the liquid, the contact angles on the resist side and the immersion unit side, as well as the dynamics of the liquid in the gap between the last lens and wafer. To optimize the performance of the immersion unit which often must be designed to work well with a wide operating range of resist coats that have different wettability, substantial investigations have been conducted to understand water leakages due to film pulling and meniscus overflow. These efforts have led to several semi-empirical models for predicting critical velocity with continuous liquid loss, which have been verified over a range of fluid properties and resist surfaces [3–5]. However, most published data have focused primarily on physical characteristics of the resist surface and the receding meniscus region adjacent to the wafer at steady state.

To maximize the critical scan speed of an immersion scanner, a good understanding of the fluid dynamics in the gap between the lens and substrate is desired. For this reason, a method for characterizing the meniscus dynamics using experimentally obtained images from two different (hydrophilic and hydrophobic) lens surfaces is developed in this work. The objective is to provide a basis for analyzing the liquid behavior and meniscus stability and for developing dynamic models to guide the design of an immersion system.

2. Experimental method and image processing

This section describes the experimental setup and the image processing steps for extracting the essential features for characterizing the transient behaviors of the immersion flow.

* Corresponding author.
E-mail address: xfu@zju.edu.cn (X. Fu).
[1] Visiting Pao Yu-Kong Chair Professor at Zhejiang University.

0167-9317/$ - see front matter © 2011 Elsevier B.V. All rights reserved.
doi:10.1016/j.mee.2011.02.045

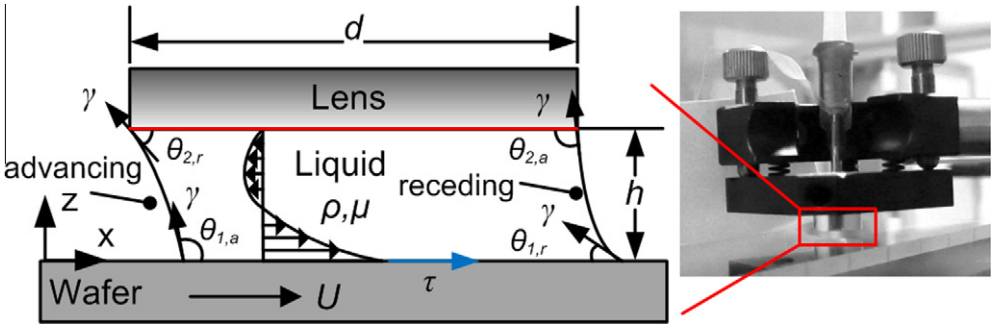

Fig. 1. Schematics illustrating the meniscus development during wafer motion.

2.1. Experimental method

As schematically illustrated in Fig. 1, the liquid (density ρ, surface tension γ, and viscosity μ) is dispensed into a gap (height h) between the lens and wafer, and drawn by the wafer at speed U. The upper surfaces of the confined liquid are the bottom of the lens and the immersion unit; for simplicity, only the lens (with diameter d) is depicted in Fig. 1. When scanning, the advancing and receding menisci (characterized by the angles, θ_a and θ_r respectively) change dynamically from their static values.

As shown in Fig. 1, the upper surface is a lens (8 mm in diameter) with a 2 mm-diameter injection hole in its center, through which purified water (Elix advantage 5, Millipore) is injected into the gap h using a syringe pump (KD Scientific, Model 200 series). The lens is mounted on a mirror bracket that can be fine tuned to ensure parallelism between the lens and the substrate (placed on a translational stage, the acceleration and velocity of which can be precisely controlled). The gap h can be adjusted via a precision micrometer and translation stage. During scanning motion, the free boundary of the confined liquid is recorded using a high-speed camera (FASTCAM-ultima APX) with a microlens. A fiber-optic cold-light source provides an auxiliary back-lighting for the flow field.

The effects of two different upper surfaces on the liquid control have been investigated; namely,

(a) quartz lens (with a *hydrophilic* surface as the projection lens model) and
(b) duraluminium alloy (Al-alloy) lens (with a *hydrophobic* surface as the immersion unit model).

The optical glass with magnesium fluoride coating is employed as the substrate which has wettability similar to that of a typical resist coated wafer.

In each trial, both the upper surface and substrate were cleansed with ethanol and then with purified water using dust-free paper before each scanning motion. Liquid was then injected incrementally until it fully filled the gap between the lens and the substrate. The translational stage was set into motion as soon as the camera began recording. The substract velocity was gradually stepped up in each trial until liquid loss occured.

2.2. Image processing

The motion was recorded at 250 fps, during which hundreds of images were obtained for each trial to provide relatively complete information for analyzing the meniscus development and fluid characteristics. Results were then statistically analyzed with the help of an image processing algorithm in MATLAB (R2009b) environment. For image analyses, the flow-field images were converted to grayscale maps (Fig. 2a), from which the following features were extracted:

(1) the aquatic cross-sectional area (Fig. 2b) in x–z plane, and
(2) the coordinate values characterizing the edges of the advancing and receding menisci.

Since the lens was stationary, the projected points of the left and right corners of the lens were chosen as references for measuring x_a and x_r respectively (Fig. 2c).

3. Results and discussion

Experiments have been carried out on the immersion tool described in Section 2.1 to study meniscus behaviors with free boundary in immersion flow field. The effects of two different (hydrophilic and hydrophobic) lens surfaces on the liquid control were investigated. Hundreds of images were analyzed to extract the fluid dynamics information for experimentally characterizing the fluid behavior in the gap, and for investigating the effects of different lens surfaces on liquid loss:

– Dynamic behaviors (Section 3.1). Experiments (with results given in Figs. 3–6) were performed on the quartz lens with a *hydrophilic* surface.

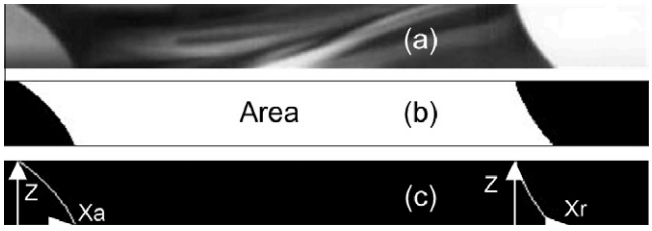

Fig. 2. Image processing. (a) Grayscale image, (b) image processed for calculating the cross-sectional area, and (c) image processed for detecting meniscus edges.

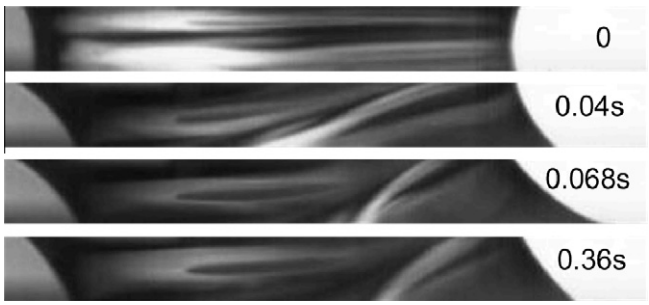

Fig. 3. Liquid behaviors with scanning velocity U = 60 mm/s (hydrophilic lens).

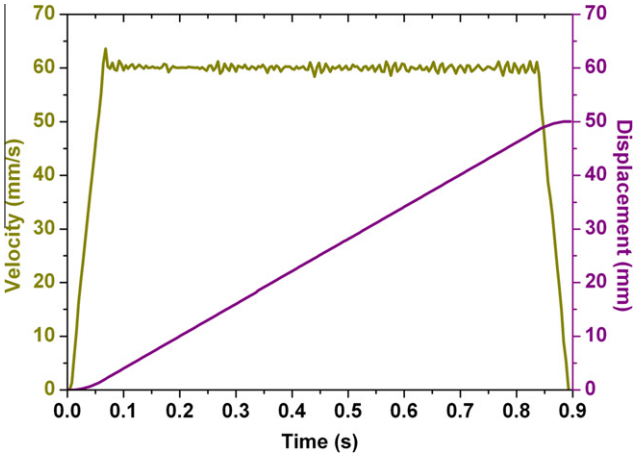

Fig. 4. Velocity and displacement profiles of the *x*-stage.

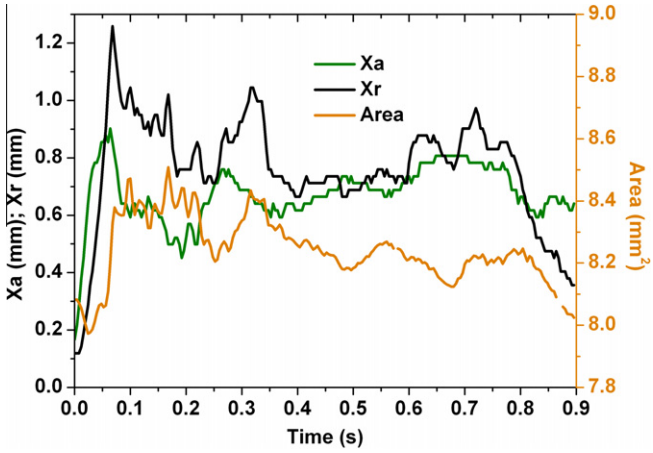

Fig. 5. Displacements (x_a and x_r) of the advancing and receding menisci, and cross-sectional area of the fluid in *x*–*z* plane during motion (hydrophilic lens, U = 60 mm/s).

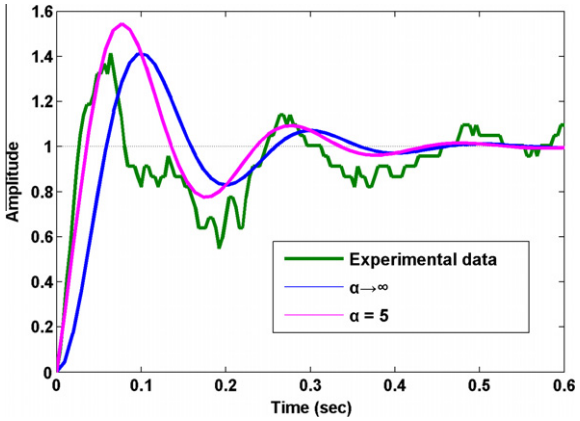

Fig. 6. Modeled displacement x_a of the advancing meniscus, $\zeta = 0.27$, $\omega_n = 32.6294$ rad/s.

– Liquid loss (Section 3.2). The effects of two different lens (*hydrophilic* and *hydrophobic*) surfaces on liquid loss were investigated, where the *hydrophilic* surface has been chosen as the basis for comparison.

3.1. Transient behaviors

Experimental results show that the liquid in the gap behaves similarly during each scanning motion when U is lower than the critical velocity beyond which liquid loss occurs. A typical set of data with the hydrophilic lens is given in Figs. 3–5 illustrating the liquid behaviors with a scanning speed of 60 mm/s. Specifically, Fig. 3 highlights four characteristic snap-shots from initial to steady state; and Fig. 5 shows the transient behaviors of the cross-sectional area and the advancing and receding menisci in response to the motion trajectory (Fig. 4) of *x*-translational stage. The following observations can be made from these results:

(1) Fig. 3 shows that as the liquid is dragged by the fictional force of the moving substrate, the advancing and receding menisci develop at the air/liquid interface (under the influence of surface tension). During the initial period (t = 0–40 ms) of the scanning motion, both the advancing and receding menisci (characterized by x_a and x_r) increase from their static values. When the advancing angle reaches its maximum (t = 60 ms), the receding meniscus x_r under traction continues to increase and peaks at t = 68 ms, which is accompanied by the decrease of the receding angle θ_r. Under the influence of surface tension, the liquid retracts to its equilibrium ($t \geqslant 0.36$ s).

(2) During the period between t = 0 and t = 0.6 s (Fig. 5), the displacement x_a of the advancing meniscus to a step change in U (neglecting the effect of short constant-acceleration) can be characterized as a second-order system transfer function of the form:

$$\frac{X_o(s)}{U(s)} = \frac{\omega_n^2[s/(\alpha\varsigma\omega_n) + 1]}{s^2 + 2\varsigma\omega_n s + \omega_n^2} \tag{1}$$

where s is a Laplace variable; ω_n is the undamped natural frequency; ζ is the damping ratio and α is a constant. Fig. 6 compares experimentally obtained x_a against those computed from (1) using step commands in Matlab, where $\zeta = 0.27$, $\omega_n = 32.6294$ rad/s and two α values ($\alpha = 5$ and $\alpha \to \infty$). The case $\alpha \to \infty$ corresponds to a standard mechanical mass-spring-damper system (without a zero); its maximum overshoot M_p and undamped natural frequency ω_n are given by Eqs. (2) and (3) respectively [6]:

$$M_p = [x(t_p) - x(\infty)]/x(\infty) = \exp(-\varsigma\pi/\sqrt{1-\varsigma^2}) \tag{2}$$

$$\omega_n = 2\pi/(T\sqrt{1-\varsigma^2}) \tag{3}$$

where the peak and steady-state displacements, $x(t_p)$ and $x(\infty)$ as well as the period T can be estimated from the experimentally obtained damped response in Fig. 5.

The discrepancy between the experimental data and those computed from the standard 2nd order system suggests that the stage applies its displacement input to the fluid through a viscous "damper"; this physical phenomenon can be accounted for by an additional derivative term ($\alpha = 5$) in the numerator. While the empirical model offers some intuitive insights into the dynamic characteristics of the immersion fluid, some differences between the model and the experimental data are somewhat expected as the lumped-parameter approach employed here generally yields only 1st order accuracy.

(3) The displacement x_r of the receding meniscus lags behind and peaks higher than x_a of the advancing meniscus. Both x_a and x_r, however, approach the same steady-state values during the period between t = 0.4 s and t = 0.6 s, beyond which they gradually increase until the stage decelerates to zero.

(4) The variations of the aquatic cross-sectional area offer flow information in the y-direction (normal to the x–z plane). The dynamic responses of the liquid area and the advancing meniscus are nearly $-180°$ out of phase. The aquatic area decreases when the x_r increment is less than the x_a increment; as a result, the liquid moves outwards (in the y-directions) from the x–z plane. On the other hand, the liquid flows back towards the x–z plane when the x_r increment is larger than x_a increment; as a result, the aquatic area increases. The free-boundary of the liquid behaves like a spring–damper pair which expands or retracts about the equilibrium state under the influence of surface tension during the scanning motion.

These above observations suggest that the oscillatory advancing meniscus and the transport lag (between the advancing and receding menisci) have a significant effect on the dynamics of receding meniscus.

3.2. Liquid loss

Experiments were conducted to examine the fluid dynamics of cases where liquid loss occured. Experimental results show that as the scanning speed increases, the advancing angle increases and receding angle decreases gradually. A typical set of data for the hydrophilic lens setup during film pulling is given in Fig. 7 that highlights several characteristic snap-shots. Fig. 8 graphs the transient responses of the cross-sectional areas and displacements of the advancing and receding menisci (in response to a similar motion trajectory shown in Fig. 4) to illustrate the process of liquid losses. When liquid loss occurs during film pulling, x_r is virtually undefined and thus eliminated in Fig. 8. Similar results for the hydrophobic lens setup are presented in Figs. 9 and 10. The followings are observations drawn from these results:

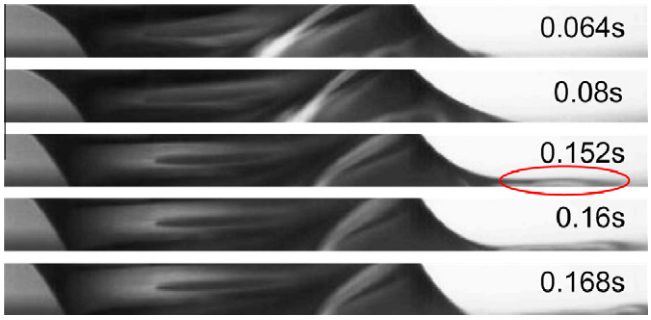

Fig. 7. Film pulling then pinched off phenomenon (hydrophilic lens, U = 65 mm/s).

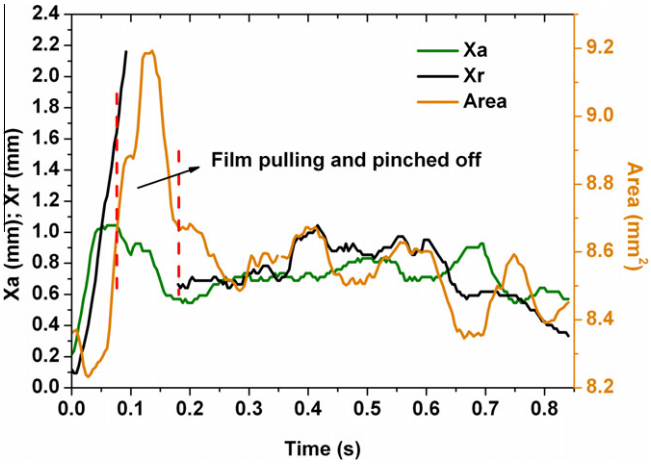

Fig. 8. Displacements (x_a and x_r) of the advancing and receding menisci, and cross-sectional area of the fluid in x–z plane during motion (hydrophilic lens, U = 65 mm/s).

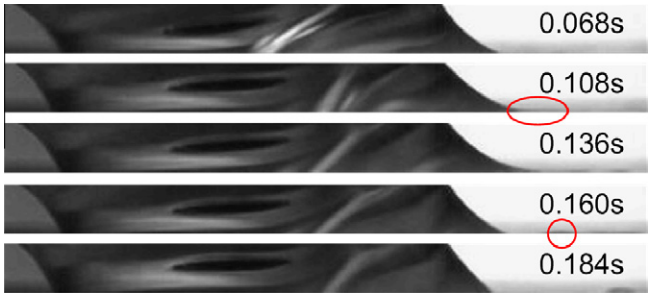

Fig. 9. Film pulling then pinched off phenomenon (hydrophobic lens, U = 45 mm/s).

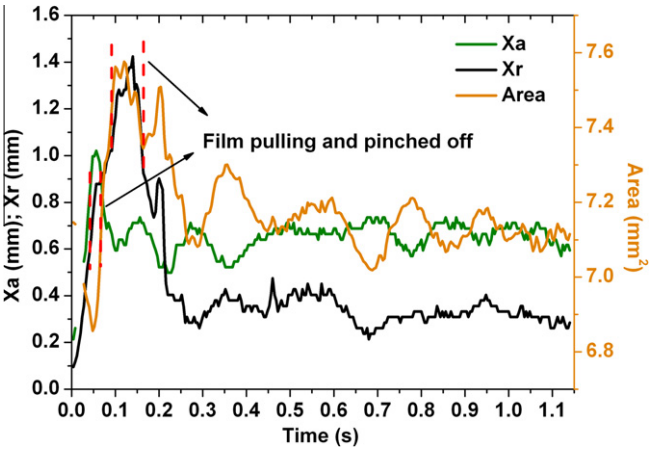

Fig. 10. Displacements (x_a and x_r) of the advancing and receding menisci, and cross-sectional area of the fluid in x–z plane during motion (hydrophobic lens, U = 45 mm/s).

(1) Fig. 7 shows liquid loss occurs with film pulling, when the balance between frictional force and surface tension forces collapses. During the initial period (t = 0–70 ms) of the scanning motion, the receding meniscus displacement (x_r) increases from static value, along with the receding angle decreasing. When the angle decreases nearly to zero (t = 80 ms), the receding meniscus is pulled into a liquid trail (t = 152 ms). Under the influence of surface tension the trail shrinks (t = 152 ms), gets pinched off (t = 160 ms), and then the liquid retracts to its new equilibrium ($t \geqslant 0.17$s) again.

(2) As illustrated in Fig. 8, a sharp elevation in the area curve (with a much higher peak value than its steady-state value) can be seen when liquid loss occurs. This suggests an abrupt liquid flow from y-direction and substantial increase of fluid in x–z plane within a short time.

(3) Once the critical scanning speed is exceeded, the phenomenon of "film pulling then pinched-off" occurs repeatedly during each trial. However, such an intermittent liquid-loss phenomenon eventually becomes continuous as the scanning speed increases beyond a certain value.

(4) The above phenomena can also be seen in the hydrophobic lens setup as shown in Figs. 9 and 10.

(5) The critical velocity of film pulling is 65 mm/s for the hydrophilic lens, and 45 mm/s for the hydrophobic lens. The results show that the meniscus adhering to the hydrophilic surface allows for a higher scanning speed than that adhering to the hydrophobic surface.

4. Conclusion

A method based on image processing techniques has been developed for characterizing the meniscus dynamics and analyzing the liquid behavior and meniscus stability in immersion lithography. This method provides a means to determine the transient responses of the meniscus position and the liquid area, from which the dynamic characteristics in the flow field and at the interfaces of air/liquid can be modeled. As characterized by a second-order system with experimental validation, the results show that the liquid free-boundary behaves like a spring–damper pair which expands or retracts about the equilibrium state under the influence of surface tension during the scanning motion.

In addition, the oscillatory advancing meniscus and the transport lag (between the advancing and receding menisci) have a significant effect on the dynamics of the receding meniscus. The model provides not only a better understanding on the development of the meniscus during scanning motion, but also a potentially useful tool to guide future designs of immersion system for reliable immersion lithography. Experimental results also suggest that the meniscus adhering to the hydrophilic surface allows for a higher scanning speed than that adhering to the hydrophobic surface. This finding offers additional physical insights into new alternatives of immersion unit designs such as creating a hybrid hydrophilic–hydrophobic surface to enclose the inside hydrophilic region with a hydrophobic surface to protect immersion liquid against leakage.

Acknowledgements

This project has been financially supported by the National Natural Science Foundation of China (91023015), Zhejiang Provincial Natural Science Foundation of China (R105008 & 1080038) and International S&T Cooperation Program of China (2008DFR70410). The authors thank Wei Wang (a visiting scholar at Georgia Tech from Huazhong University of Science and Technology) for providing image processing algorithms for analyzing experimental data.

References

[1] B.W. Smith, A. Bourov, H. Kang, F. Cropanese, Y. Fan, N. Lafferty, L. Zavyalova, J. Microlith. Microfab. Microsyst. 3 (44) (2004) 44–51.
[2] W. Chen, X. Fu, J. Zou, H. Yang, X. Ruan, G. Gong, Microelectron. Eng. 87 (5–8) (2010) 1070–1073.
[3] S. Schuetter, T. Shedd, K. Doxtator, G. Nellis, J. Microlith. Microfab. Microsyst. 5 (2) (2006) 023002.
[4] H.B. Burnett, Master's thesis, University of Wisconsin–Madison, Madison, Wisconsin, 2005.
[5] S. Schuetter, T. Shedd, G. Nellis, J. Micro/Nanolith MEMS MOEMS 6 (2) (2007) 023003.
[6] M. Driels, Linear Control Systems Engineering, MCGraw-Hill College, New York, 1996.